Welding in the World (2019) 63:349–363
https://doi.org/10.1007/s40194-018-00697-7

RESEARCH PAPER

Fatigue strength of thermal cut edges—influence of ISO 9013 quality groups

Paul Diekhoff[1] · J. Hensel[1] · Th. Nitschke-Pagel[1] · K. Dilger[1]

Received: 2 March 2018 / Accepted: 12 December 2018 / Published online: 7 January 2019

Abstract
The use of high strength steels has gained importance due to the interest in effective light steel constructions. Besides the well-designed weld seams, free cutting edges gain technical and economic relevance as locations for potential fatigue cracks. In this investigation, fatigue tests were carried out on 8-mm- and 20-mm-thick samples with a minimum yield strength ranging from 355 to 960 MPa at a stress ratio of $R = 0.1$. The cutting methods used were oxygen, plasma, and laser cutting. The surface roughness, hardness profile, and residual stresses were measured to classify the specimens into quality groups according to ISO 9013. Most of the specimens are classified in the quality groups 2 and 3. A slight tendency can be seen that the fatigue strength decreases with an increasing roughness value. Increasing local hardness values at the cut edges also have a minor negative influence on the fatigue strength. No positive impact was observed for increasing tensile strength on the fatigue strength. With higher surface roughness values, larger notches exist, the crack initiation starts early, and the fatigue strength decreases.

Keywords Thermal cutting · Fatigue strength · Surface roughness · Cut edge · Surface quality

1 Introduction

Designing welded constructions, the fatigue strength reducing effects of the weld seams is taken into account at an early stage. Therefore, welds are placed in lowly stressed areas and conventional post-treatment methods, for example grinding, are used. As a result, free cutting edges gain technical and economic relevance as locations for potential fatigue cracks.

Depending on the process and the cutting parameters used, thermal cutting technologies produce different execution qualities at the cutting edge. The requirements for the quality characteristics of the components are for instance defined according to EN 1090 [1] and ISO 9013 [2] respectively. Especially, the surface roughness is a factor governing the fatigue strength of thermal cut edges. In addition, for different steel grades, a maximum permitted hardness value is required. High cutting speeds related with high cooling rates show that these hardness values are often exceeded.

In this investigation, fatigue tests were carried out on thermal cutting edges in different execution qualities with a constant force amplitude at a stress ratio $R = 0.1$. The tested specimens were made from 8-mm- and 20-mm-thick plates with a minimum yield strength ranging from 355 to 960 MPa. The cutting methods used were oxygen cutting, plasma cutting, and laser cutting. All samples were characterized in terms of hardness, roughness, and other quality characteristics according to EN 1090 and ISO 9013. Furthermore, the residual stresses were measured and correlations between fatigue strength, roughness, hardness, and residual stresses for various cut materials were shown. In addition, the positive impact for increasing tensile strength on the fatigue strength was observed and after which cut edge quality the impact exists.

Recommended for publication by Commission XIII - Fatigue of Welded Components and Structures

✉ Paul Diekhoff
p.diekhoff@tu-braunschweig.de

[1] Institute of Joining and Welding, University of Braunschweig, Langer Kamp 8, 38106 Braunschweig, Germany

2 Influencing factors on fatigue strength

The fatigue behavior of steel structures and components depends on various factors such as the material used, the geometric shape of the component, and the manufacturing process. The fatigue strength is determined by the following parameters and they interact with each other:

- Load (loading conditions)
- Construction (design)
- Material
- Manufacturing
- Environmental conditions

The operational load can usually not be affected due to the general conditions in use. On the other hand, the structural design can influence the local stresses of the component and the maximum load is considered by selection of suitable materials and productions. For a correct dimensioning of components it is not sufficient to know the material properties such as tensile strength R_m, yield strength YS, elongation at break, necking and notched bar impact work alone. Also the constructive design and the production have an influence on fatigue strength [3]. In the following, the influence factor material, surface roughness, and residual stresses will be discussed more in detail.

2.1 Material

The fatigue strength of unnotched and polished specimens depends primarily on the tensile strength [4, 5]. The tensile strength is also in proportion to the hardness. The relation can be described by $R_m \sim 3.2$ H for S355 steels, R_m in N/mm^2, and H in HV [6]. Especially the surface condition is responsible for the fatigue strength. The trend of the steels is explained by the micro-notch effect of carbide inclusions, which occur in tempered martensite [7].

The fatigue strength of unnotched and polished material samples can be increased up to a certain limit by increasing the tensile strength and yield strength. According to Dahl, the following measures can be used [8]:

- Grain refinement: As the grain size decreases, the yield strength increases and the ductility improves
- Mixed crystal formation: Alloys have a modified microstructure, which increases the tensile strength.
- Precipitation hardening: Small distributed hard particles of a second phase reduce the dislocation movement and increase the tensile strength and the fatigue limit.
- Strain hardening: The material solidifies by cold forming, but loses at the same time the remaining ductility

Wu and Radaj pointed out that the fatigue strength of unnotched and polished specimens is not the focus of interest for designing parts. Instead of fatigue life in finite fatigue cycle regions and operational strength including notch effect and crack propagation is of higher importance [9].

2.2 Surface roughness

The dependency of the material parameters (R_m: tensile strength, R_e: yield strength) and the surface roughness is very small under static load. In contrast, the condition of the surface is significant to characteristic values of the fatigue strength. The influence of the roughness of technical surfaces on fatigue strength is predominantly an influence of the stress increase due to the microgeometric surface profile compared to the micro notch-free polished samples [7]. The maximum stress usually occurs at the surface, the surface profile causes superficial microcracking due to micro-notch effect and the surfaces are exposed to corrosion, which leads to micro cracks as well. The influence of the surface can be taken into account by a correction factor, next to others for instance according to the FKM guidelines. [10]

2.3 Residual stress

Residual stresses are internal stresses in components without the effect of external forces or thermal gradients. They are caused by heterogeneous plastic strains from hindered shrinkage during cooling and/or phase transformation. Residual stresses are generated during the production of components by casting, rolling, welding and thermal cutting, coating, surface treatment, hardening, and quenching. Particularly during welding, high residual stresses may occur due to the concentrated heat input on the component. Surface layer residual stresses have a big effect on the fatigue strength because cracks usually start on the specimen surface. The influence on the fatigue strength is very complex. During cyclical fatigue tests, residual stresses may change and can be relaxed. It is known that the influence in high-strength materials is particularly high because of the higher residual stresses stability; the fatigue strength increases by compressive residual stresses and is reduced by tensile residual stresses [7, 11].

3 Fatigue strength of thermal cut edges

Conventional thermal cutting technologies produce different execution qualities at the cutting edge. The theoretical relation between steel strength and fatigue strength can be shown in a so-called Kitagawa diagram [11], as illustrated in Fig. 1. It shows the influence of the surface defect size on the fatigue strength. For components with sufficiently large defects, the fatigue strength of the component is characterized by the crack propagation phase. With such defect sizes, the fatigue strength does not increase with the tensile strength. The execution quality in terms of surface roughness (or “defect size”) directly influences the local stress level and therefore the expected lifetime of the component. Component lifetime is governed by crack growth in case of large defects and by crack initiation in case of small defects. Crack initiation is affected by the hardness respectively tensile strength resulting in an increase of fatigue strength with increasing tensile strength in the presence of small defects. A higher material strength therefore leads to a higher fatigue strength of the

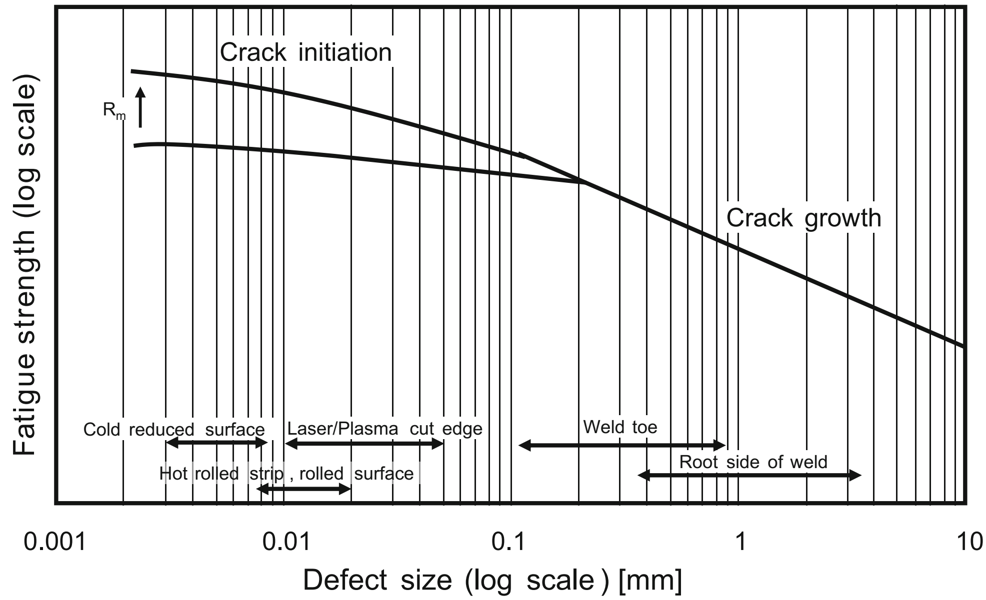

Fig. 1 Schematic Kitagawa diagram showing the influence of the defect size on fatigue strength of different steel strengths (according to Sperle [11]).

component due to the suppressed dislocation movement. In general, for thermal cutting edges, the fatigue strength should increase with tensile strength if the defect (or surface roughness) is smaller than the corresponding limit value.

The influence of thermal cutting edges and their different qualities on fatigue strength have been discussed several times, for example, by Sperle [11], Remes et al. [12], and Stenberg et al. [13]. Sperle conducted fatigue tests with a comprehensive range of steel grades (yield strengths from 240 to 900 MPa) on 6-mm- and 12-mm-thick specimens. The specimens were thermally cut by gas, plasma, and laser. He found out that the fatigue strength increases with the steel grade depending on the surface roughness. The investigation compared also the plasma and laser cut edges with machined edges. Sperle determined that the fatigue strength rises with increasing tensile strength depending on the roughness. The increase of the fatigue strength in all cases is comparable, which was explained by the consistently small roughness depth.

Another study was made by Remes et al. [12]. They used 15-mm- and 17-mm-thick specimens, which were plasma cut and considered three series: first untreated, second ground, and third ground + sandblasted. The surface roughness, hardness, and residual stresses were determined out for the rolled plate surface and specimen cut edge. Fatigue tests on specimens were conducted, which had yield strengths of 460 MPa or 690 MPa, with different surface treatments. The investigation shows that post treatments increase the fatigue strength of high strength steel due to the reduced surface roughness and induced compressive residual stresses. Stenberg et al. [13] studied the influence of surface roughness on the fatigue strength in high strength steels (S700 and S960) of 6-mm- and 16-mm-thick specimens. They were thermally cut using oxygen, plasma, laser, and waterjet cutting. Surface roughness was measured and classified in the four quality ranges according to the ISO 9013 standard for thermal cutting quality tolerances (Table 1). It was used to assess the produced quality of the thermally cut edges. The testing proved an increased fatigue strength compared to the conservative international guidelines [14]. However, the examinations do not cover all quality ranges. At this point, the question arises, up to which conventional cutting edge quality fatigue strength increases with higher strength of material. The execution quality, for example according to ISO 9013, of the material or different cutting processes in the guidelines is not considered yet.

4 Experiment

4.1 Materials and test samples

The fatigue strength of different thermal cut edges of varying steel grades with a yield strength of 355 MPa up to 960 MPa was analyzed. Therefore, axially loaded dog-bone specimens were considered as shown in Fig. 2. In the center, the specimens had a parallel length of 20 mm to determine the critical cross section.

Table 1 Surface roughness quality ranges according to ISO 9013

Quality range	Mean height of the profile, R_z [μm]
1	$10 + 0.6 \cdot t$
2	$40 + 0.8 \cdot t$
3	$70 + 1.2 \cdot t$
4	$110 + 1.8 \cdot t$

t, plate thickness [mm]

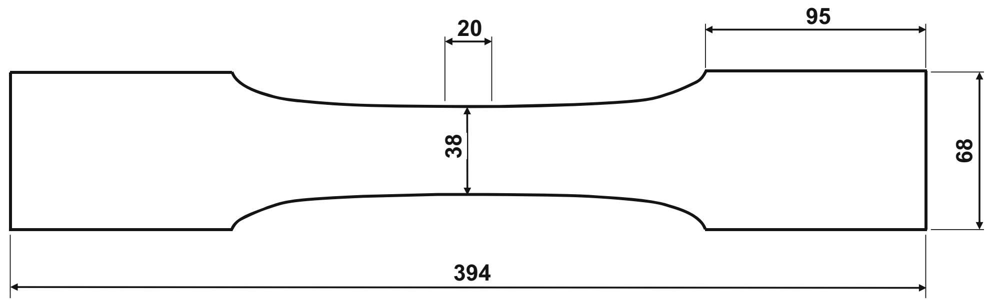

Fig. 2 Dimensions of the dog-bone specimen for fatigue test in millimeters

The experimental program covered five different steel grades with a wide range of mechanical properties:

– S355M: Thermomechanically rolled weldable fine grain structural steels with minimum yield strength of 355 MPa and a Carbon Equivalent Value (CEV) less than 0.39, EN 10025-4, [15]. Samples were cut from an 8-mm-thick plate.
– S355N: Normalized rolled weldable fine grain steels with a minimum yield strength of 355 MPa and a Carbon Equivalent Value less than 0.43, EN 10025-3, [16]. Samples were cut from a 20-mm-thick plate.
– S460M: Thermomechanically rolled weldable fine grain structural steels with minimum yield strength of 460 MPa and a Carbon Equivalent Value (CEV) less than 0.43, EN 10025-4, [15]. Samples were cut from an 8-mm-thick plate.
– S690Q: Quenched and tempered high strength steel with a minimum yield strength of 690 MPa and a Carbon Equivalent Value less than 0.65, EN 10025-5, [17]. Samples were cut from an 8-mm- and 20-mm-thick plate.
– S960Q: Quenched and tempered high strength steel with a minimum yield strength of 960 MPa and a Carbon Equivalent Value less than 0.82, EN 10025-5, [17]. Samples were cut from an 8-mm-thick plate.

Figure 3 shows the experimentally determined CEV’s of materials tested as well as the quality group of the produced cutting edges according to the roughness value of ISO 9013. The corresponding thermal cutting process, thickness *t*, cutting speed *v*, and the tensile properties (yield strength YS, tensile strength R_m) are summarized in Table 2.

Besides the various steel strength, the specimens were cut using oxy-fuel, plasma, and laser cutting processes. The conditions for each specimens were untreated and defined “as cut” without any posttreatment processes used, e.g., grinding and sandblasting. All sets with 20-mm thickness were cut using two cutting speeds to generate an individual cut-edge quality. Additionally, laser cutting speed was reduced using a 10-Hz pulsed laser for two steel grades (S355M, S690Q). A

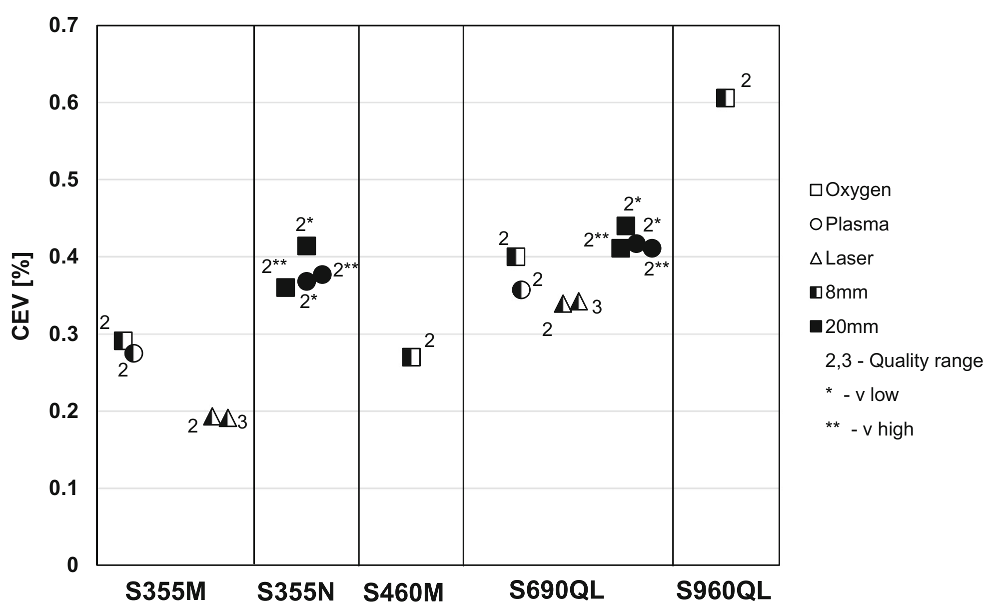

Fig. 3 Carbon Equivalent Value of materials tested with the quality range according to the DIN EN ISO 9013

Table 2 Tensile properties of steels and tested cutting technologies

No.	Steel grade	Cutting process	*t* [mm]	*v* [m/min]	Yield strength [MPa]	Tensile strength [MPa]	Number specimens tested
1	S355M	Oxygen	8	0.60	393	492	10
2	S355M	Plasma	8	3.42	393	492	10
3	S355M	Laser	8	0.90	440	517	10
4	S355M	Laser	8	1.10	440	517	10
5	S355N	Oxygen	20	0.39	378	564	10
6	S355N	Oxygen	20	0.42	378	564	10
7	S355N	Plasma	20	1.30	378	564	10
8	S355N	Plasma	20	1.43	378	564	10
9	S460M	Oxygen	8	0.60	555	648	10
10	S690Q	Oxygen	8	0.60	822	867	10
11	S690Q	Plasma	8	3.42	822	867	10
12	S690Q	Laser	8	0.90	759	797	10
13	S690Q	Laser	8	1.10	759	797	10
14	S690Q	Oxygen	20	0.39	820	861	10
15	S690Q	Oxygen	20	0.42	820	861	10
16	S690Q	Plasma	20	1.30	820	861	10
17	S690Q	Plasma	20	1.43	820	861	10
18	S960Q	Oxygen	8	0.60	1011	1058	10

total amount of 180 fatigue specimens were tested, which were at least 10 samples per test series.

Notice that this study investigates the fatigue performance of thermally cut edges using typical industry-related cutting parameters. It does not aim to improve the cutting parameters for each thermally cutting method.

4.2 Characterizing edge conditions

Surface roughness measurements were made on the specimens according to ISO 4288 [18]. The measurements were done for the rolled plate surface and the cut edge surface along three lines (Fig. 4). The tests were carried out with the MarSurf M 400 surface measuring instrument using the profile method over the length of 17.5 mm. The average of the five highest peaks and lowest valleys, R_z, and the arithmetical average, R_a, were defined. Cross sections have been cut from the dog-bone specimens by using a water-cooled abrasive cutter to analyze the hardness in the heat-affected zone (HAZ) of thermally cut edges. Vickers hardness measurements were made for each series according to ISO 6507 [19]. As shown in Fig. 4, the hardness depth profiles of both sides of the samples were carried out as well as measurements in the base material (BM). The residual stresses were measured on the cut edge of all series using the X-ray diffraction technique (XRD) (Fig. 4). For the XRD-experiments, a ψ-diffractometer was used. The longitudinal residual stresses were calculated from the {211}-Fe diffraction lines determined at 15 ψ-angles with help of the $\sin^2 \psi$-method.

Figure 5 shows exemplary the cut surface of steel S355M by using oxygen, plasma, and laser. At the top of each figure, there is the upper edge and at the bottom, there is the lower edge of the cut surface. It can be observed that oxygen cutting implicates a lot of slag and scale, which stick to the edge. It

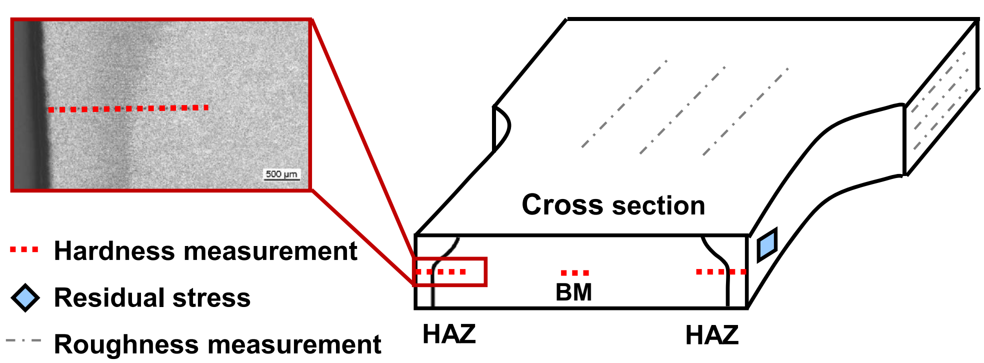

Fig. 4 Locations of hardness and residual stress measurements

Fig. 5 Cut surfaces of steel S355M (8 mm thick): **a** oxygen cutting, **b** plasma cutting, and **c** laser cutting

provides a cut surface with varying roughness. Plasma cutting creates the cut surface with the lowest roughness, while laser cutting generates surfaces with the highest roughness value. No other defects on the surfaces are visible.

The corresponding roughness measurements and allowable ranges, according to EN 9013, are shown in Fig. 6. It demonstrates the arithmetic mean of surface roughness R_a as a function of arithmetical peak-to-peak average roughness R_z for different cutting technologies and steel strengths (thickness 8 mm). The different quality groups according to Table 1 for 8-mm-thick specimens are also shown. All steel grades have different symbols (cycle—S355M, square—S460M, triangle—S690Q, diamond—S960) and the cutting technologies have various colors (red—oxygen, blue—plasma, green—laser). All measurements can be classified in range 2 and range 3. The mean values of the specimens go up to $R_z = 43.8$ (range 2) for oxygen, $R_z = 26.5$ (range 2) for plasma, and $R_z = 35.67$ for continuous laser (range 2) or $R_z = 67.08$ for a 10-Hz pulsed laser (range 3).

The different cutting technologies affected the material close to the cut edge, as shown schematically in Fig. 7. Cutting speeds as well as the plate thickness related with the cooling rates have an influence on the size of the heat-affected zone (HAZ). The CEV of the steel grades determine the possible maximum hardness. Figure 7 shows hardness measurements on the cross section according to Fig. 4 of three exemplary specimens (S355M, 8 mm; S355N, 20 mm, S690Q, 8 mm). The curves are plotted for each cutting technology oxygen, plasma, and laser. All measurements were done approx. 2 mm from both sides of the cross section into the unaffected base material. Concerning the hardness measurements, the HAZ is less than 1 mm wide. The curve on the left and right side is essentially identical of each set. Higher strength steels coming up with higher CEV implicate higher hardness values at the thermally cut edges. Comparing the cutting processes, plasma cutting achieves the highest hardness value. No hardness increase is observed at the oxygen cut S335M. The hardness gradient for 20-mm-thick plates is lower and the hardness curve drops slower with increasing edge distance. The rapid change in the hardness profile of 8-mm-thick plates indicates a very heat-affected zone. Laser cut specimens have such a small HAZ that only one hardness measurement point fit into it. Regardless of the steel grade, the maximum hardness value is between 200 HV 0.1 and 510 HV 0.1. It implicates a relatively increased hardening compared to the base material from 10 to 170%. Consequently, hardening occurs locally resulting in increased ultimate strength of the HAZ, cf.

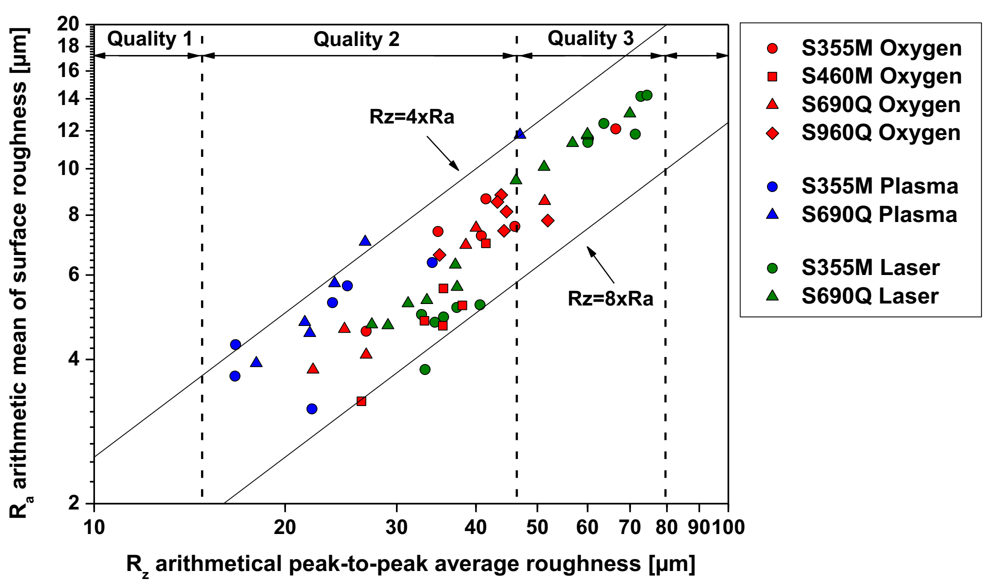

Fig. 6 Arithmetic mean of surface roughness R_a as a function of arithmetical peak-to-peak average roughness R_z for different cutting technologies and steel strengths (8 mm thick)

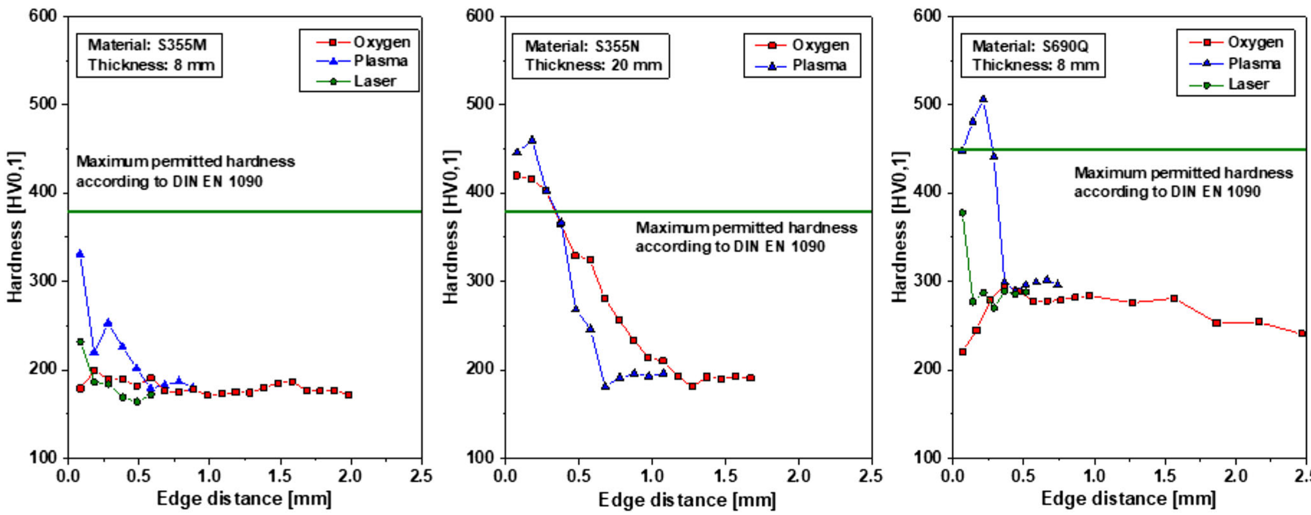

Fig. 7 Hardness measurements on the cross section of three different specimens (S355M, 8 mm; S355N, 20 mm, S690Q, 8 mm)

Figure 9. The maximum permitted hardness values according to DIN EN 1090 are partly exceeded.

4.3 Fatigue tests

All fatigue tests were performed on a 250 kN or 600 kN hydraulic testing machine using cyclic tensile tests with a stress ratio $R = 0.1$ following the recommendations of DIN 50100 [20]. The test frequency was 10–20 Hz, depending on the load level of each test. The main fatigue strength was determined in the life range of 1×10^5 to 2×10^6 cycles. The run-out point was defined at five million cycles. The tests were stopped after complete failure of the specimen. The fracture surface was analyzed to identify the location of crack initiation. Therefor, macroscopic images of all fracture pattern after testing were made.

5 Results and discussion

All individual test results are summarized in Table 3. Besides the steel grade, the cutting technology and the plate thickness the table shows the quality characteristics of the cut edge: the surface roughness, the local hardness, and the residual stresses. Furthermore, the fatigue strength with a probability of survival of $P_{OS50\%}$ for one million and two million load cycles are given. No run outs are included in the evaluation. The analysis is based on DIN 50100 with S-N curves of the form $\log N = \log C - k \log \Delta\sigma$ using simple linear regression in the direction of N. N is the number of cycles at failure, $\Delta\sigma$ is the applied stress rage, $\log C$ is the intercept of the fitting curve with the y-axis, and k is the slope of the fitting curve. The nominal stress concept was used.

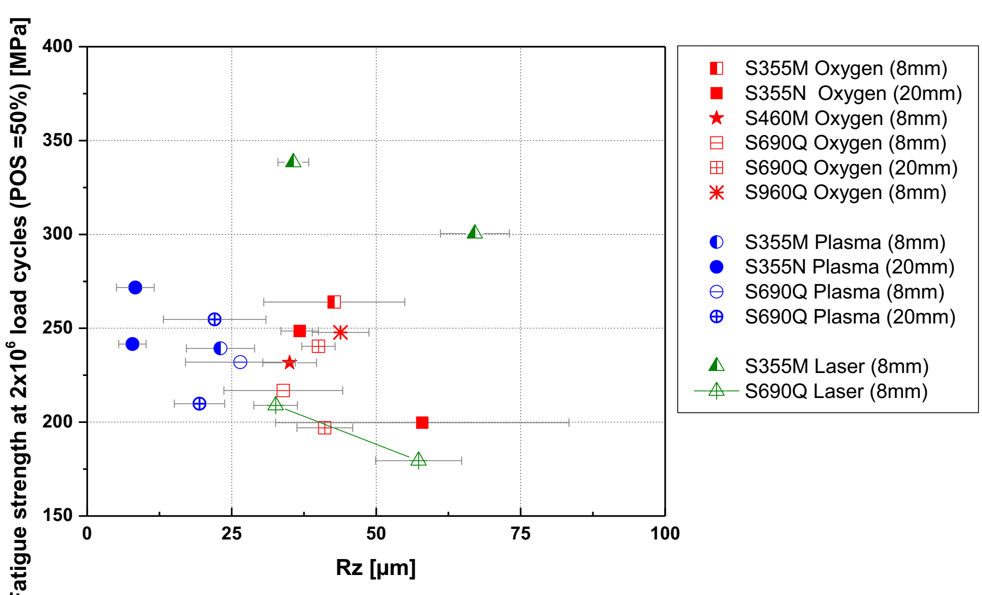

Fig. 8 Fatigue strength at 2×10^6 load cycles (POS = 50%) as a function of arithmetical peak-to-peak average roughness R_z

Table 3 Summarized results of investigations

No. –	Steel grade –	Cutting technology –	t [mm]	Surface roughness cut edge [µm]	Quality range	Local hardness of the cut edge [HV]	Residual stresses cut edge [MPa]	Fatigue strength $P_{OS50\%}$ for 1E6 [MPa]	Fatigue strength $P_{OS50\%}$ for 2E6 [MPa]
1	S355M	Oxygen	8	43 ± 12	2	197 ± 9	15 ± 12	297	264
2	S355M	Plasma	8	23 ± 6	2	281 ± 10	208 ± 28	273	239
3	S355M	Laser	8	36 ± 3	2	225 ± 6	728 ± 28	358	338
4	S355M	Laser	8	67 ± 6	3	285 ± 7	320 ± 26	322	300
5	S355N	Oxygen	20	37 ± 3	2	312 ± 12	− 204 ± 25	279	249
6	S355N	Oxygen	20	58 ± 20	3	364 ± 10	− 137 ± 29	238	200
7	S355N	Plasma	20	8 ± 3	1	442 ± 5	− 36 ± 13	296	272
8	S355N	Plasma	20	8 ± 2	1	436 ± 5	− 16 ± 7	269	242
9	S460M	Oxygen	8	35 ± 5	2	202 ± 7	68 ± 12	278	232
10	S690Q	Oxygen	8	34 ± 10	2	257 ± 7	315 ± 10	267	217
11	S690Q	Plasma	8	27 ± 10	2	425 ± 8	39 ± 25	277	232
12	S690Q	Laser	8	33 ± 4	2	314 ± 5	540 ± 25	256	209
13	S690Q	Laser	8	57 ± 10	3	385 ± 6	147 ± 11	226	179
14	S690Q	Oxygen	20	40 ± 3	2	377 ± 9	− 127 ± 22	283	240
15	S690Q	Oxygen	20	41 ± 5	2	398 ± 11	− 400 ± 13	240	197
16	S690Q	Plasma	20	22 ± 9	1	382 ± 10	99 ± 7	298	255
17	S690Q	Plasma	20	19 ± 4	1	396 ± 7	100 ± 8	266	210
18	S960Q	Oxygen	8	44 ± 5	2	283 ± 6	140 ± 9	287	248

Concerning the fatigue tests, Figs. 8, 9, and 10 show fatigue strength at 2E6 ($P_{OS} = 50\%$) cycles as a function of different quality characteristics of the specimens. The results are shown for the different steel grades S355M, S355N, S460M, S690Q, and S960Q, as well as for the various cutting technologies oxygen, plasma, and laser. In addition, the two plate thicknesses 8 mm and 20 mm were taken into account.

Figure 8 shows the fatigue strength at 2×10^6 load cycles (POS = 50%) as a function of arithmetical peak-to-peak average roughness R_z. Oxygen cut edges are marked red with

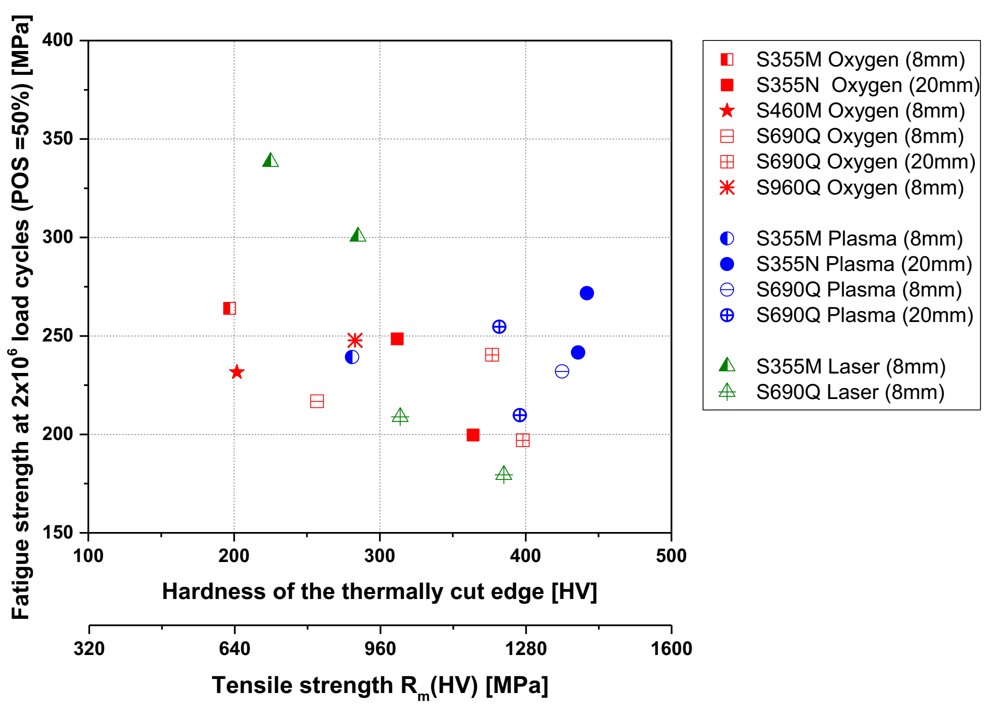

Fig. 9 Fatigue strength at 2×10^6 load cycles (POS = 50%) as a function of hardness value of thermally cut edges and as a function of converted tensile strength values using $R_m = \text{HV} \times k$, with $k = 3.2$

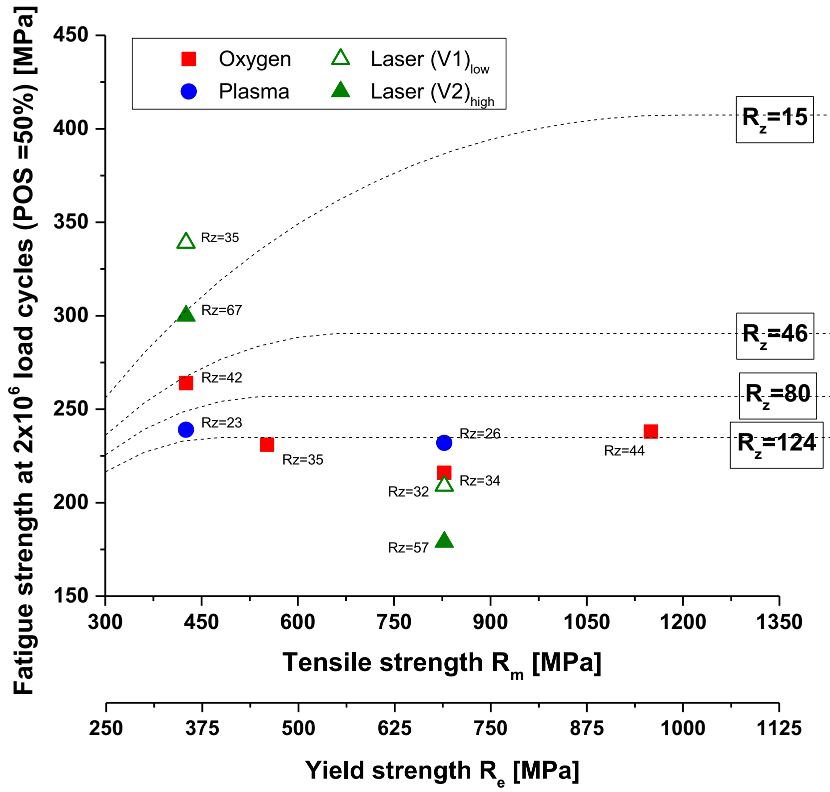

Fig. 10 Fatigue strength at 2×10^6 load cycles (POS = 50%) as a function of tensile strength and as a function of yield strength (according to Sperle [11])

different symbols for each steel grade and plate thickness. The plasma cut edges are blue and the laser cut edges are green tagged. Connected values have the same material properties using the same cutting method but different cutting speeds. It can be observed that the cutting technologies generally provide average roughness between 7 μm and 67 μm. Plasma cutting generates the lowest roughness while laser cutting resulted in the highest value depending on the cutting parameters used. Intermediate roughness values provided the oxy-fuel cutting. Furthermore, the plasma cut specimens with a thickness of 8 mm for example have average roughness values of $R_z = 23$ μm and have lower fatigue limits compared to laser cut specimens same size with three times higher average roughness values of $R_z = 67$ μm. A general slight tendency can be seen that the fatigue strength decreases with an increasing roughness value, but the steel grade and the cutting process must be considered (Tables 4 and 5).

Fatigue strength at 2×10^6 load cycles (POS = 50%) as a function of local hardness value of thermally cut edges is illustrated in Fig. 9. Also, an additional *x*-axis is integrated for converted tensile strength values using $R_m = k \times \mathrm{HV}$, with $k = 3.2$. For very mildly-notched samples, one expects an increase of fatigue strength with increasing tensile strength. However, the maximum permitted hardness is limited in DIN EN 1090, regarding that the hardness may have a negative influence on the fatigue strength because of the material embrittlement. Comparing the results, it cannot be concluded that the fatigue performance is better for higher values of local hardness at the cut edge. Rather a tendency of decreasing fatigue strength with increasing hardness values is shown.

According to Sperle [11], the fatigue strength at 2×10^6 load cycles (POS = 50%) as a function of tensile strength R_m for 8-mm-thick specimens is shown in Fig. 10. A second *x*-axis is added for the related yield strength, which Sperle compared in his study (set to 1:1.2) [11]. He observed a clear influence of steel strength on fatigue strength for specimens with machined, laser cut and plasma cut edges. He investigated a fatigue strength baseline according to the roughness of the cut edges. The limit lines which define range 1 to 4 follows his baseline converted to the plate thickness used corresponding to DIN EN ISO 9013. No positive influence of the tensile strength on the fatigue strength was found in this investigation. Oxygen and plasma cut edges show a similar fatigue strength value for different steel strength. However, laser cut edges have lower fatigue strength with higher steel strength. Comparing, the S355M laser cut edges achieved the highest fatigue strength limit, oxygen cutting provided intermediate performances, and plasma cutting the lowest value (Figs. 11, 12, and 13).

6 Conclusions

This document investigated experimentally the influence of the quality characteristics according to ISO 9013 on the fatigue strength of thermal cut edges. Fatigue tests were conducted on thermal cut edges in different execution qualities with constant amplitude loads at a stress ratio $R = 0.1$. Various steel strengths ranging from 355 to 960 MPa and with a plate thickness of 8 mm and 20 mm were considered. The cutting methods used were oxy-fuel cutting, plasma cutting, and laser cutting. All samples were characterized in terms of hardness, roughness, and residual stresses.

Fatigue strengths of specimens depend on the cutting technologies. A general slight tendency can be seen that the fatigue strength decreases with an increasing roughness value, but the steel grade and the cutting process must be considered.

Contrary to expectation, increasing local hardness values at the cut edges also have no positive influence on the fatigue strength. The surface hardening exists just in very thin layers and the material embrittlement can increase the notch sensitivity.

There was no positive impact observed for increasing tensile strength on the fatigue strength. Oxygen and plasma cut edges showed a similar fatigue strength value for different steel strength, whereby the laser cut edges have a lower fatigue strength with higher steel strength. Therefore, the notch sensitivity increases for high strength steels. Due to the high surface roughness, large notches exist and are associated with high stress concentrations where the crack initiates.

ISO 9013 classifies the quality cut edges into four different groups. According to these quality groups, no specific prediction about the fatigue limit can be made. Most of the specimens are classified in the quality group 2, which has the high roughness value range from 15 to 46 μm. Therefore, the fatigue limits can change for various steel grades and cutting technologies in one single quality group. In order to make a statement about the fatigue strength, the standard has to be specified and the steel strength as well as the cutting process has to be considered.

Funding information The presented investigations were supported by the Arbeitsgemeinschaft industrieller Forschungsvereinigungen (AiF) in the project 18.789N "Bedeutung der Qualitätsmerkmale freier Schnittkanten nach DIN EN 1090 für deren Schwingfestigkeit unter Berücksichtigung von Eigenspannungen."

Appendix

Table 4 Fatigue test results and SN curve data

Material	Cutting method	Plate thickness [mm]	Edge condition	Stress ratio R	Number of specimens	Run outs	Slope	Log *C*	SD	FAT (1E6) 50%	FAT (2E6) 50%	FAT (2E6) 97.5% Ts 1:1.5 Haibach
S355M	Oxygen	8	As cut	0.1	12	0	5.84	20.43	0.13	297	264	193
S355N	Oxygen	20	As cut	0.1	12	1	6.02	20.72	0.15	279	249	182
S355N	Oxygen	20	As cut, *v* high	0.1	11	1	3.91	15.30	0.10	238	200	146
S355M	Plasma	8	As cut	0.1	13	2	5.21	18.69	0.08	273	239	175
S355N	Plasma	20	As cut	0.1	11	2	8.13	26.09	0.07	296	272	199
S355N	Plasma	20	As cut, *v* high	0.1	8	1	6.46	21.69	0.13	269	242	177
S355M	Laser	8	As cut	0.1	10	2	12.35	37.54	0.14	358	338	248
S355M	Laser	8	As cut, puls	0.1	9	1	9.81	30.60	0.15	322	300	220
S460M	Oxygen	8	As cut	0.1	10	1	3.78	15.24	0.06	278	232	170
S690QL	Oxygen	8	As cut	0.1	13	1	3.35	14.12	0.15	267	217	159
S690QL	Oxygen	20	As cut	0.1	9	1	4.28	16.48	0.04	283	240	176
S690QL	Oxygen	20	As cut, *v* high	0.1	9	1	3.49	14.31	0.08	240	197	144
S690QL	Plasma	8	As cut	0.1	9	1	3.90	15.53	0.07	277	232	170
S690QL	Plasma	20	As cut	0.1	8	1	4.44	16.99	0.11	298	255	187
S690QL	Plasma	20	As cut, *v* high	0.1	9	1	2.90	13.04	0.08	266	210	154
S690QL	Laser	8	As cut	0.1	13	2	3.41	14.20	0.05	256	209	153
S690QL	Laser	8	As cut, puls	0.1	12	1	3.03	13.14	0.12	226	179	132
S960QL	Oxygen	8	As cut	0.1	10	1	4.75	17.68	0.21	287	248	182

Table 5 Raw data

Test specimen [index]	Load ratio [−]	Nominal stress range [MPa]	Fatigue life [cycles]
S355_A_8_01	0.1	378	257,488
S355_A_8_02	0.1	378	271,009
S355_A_8_03	0.1	378	301,023
S355_A_8_04	0.1	342	299,207
S355_A_8_05	0.1	342	552,562
S355_A_8_06	0.1	342	386,736
S355_A_8_07	0.1	306	687,346
S355_A_8_08	0.1	306	718,035
S355_A_8_09	0.1	306	803,485
S355_A_8_10	0.1	270	1,681,284
S355_A_8_11	0.1	270	1,202,510
S355_A_8_12	0.1	270	3,720,270
S355_P_8_01	0.1	378	186,313
S355_P_8_02	0.1	378	167,733
S355_P_8_03	0.1	378	168,848
S355_P_8_04	0.1	342	296,871
S355_P_8_05	0.1	342	247,063
S355_P_8_06	0.1	342	386,192
S355_P_8_07	0.1	306	679,047
S355_P_8_08	0.1	306	749,810
S355_P_8_09	0.1	306	619,227
S355_P_8_10	0.1	270	5,000,000
S355_P_8_11	0.1	270	756,423
S355_P_8_12	0.1	270	1,045,573
S355_P_8_13	0.1	252	5,000,000
S355_L_8_01	0.1	396	251,926
S355_L_8_02	0.1	396	297,990
S355_L_8_03	0.1	378	507,452
S355_L_8_04	0.1	378	1,077,419
S355_L_8_05	0.1	378	454,739
S355_L_8_06	0.1	360	5,000,000
S355_L_8_07	0.1	360	639,413
S355_L_8_08	0.1	360	5,000,000
S355_L_8_09	0.1	414	139,400
S355_L_8_10	0.1	414	169,439
S355_L_8_PULS_01	0.1	396	84,611
S355_L_8_PULS_02	0.1	378	261,235
S355_L_8_PULS_03	0.1	378	290,594
S355_L_8_PULS_04	0.1	360	343,733
S355_L_8_PULS_05	0.1	360	435,484
S355_L_8_PULS_06	0.1	342	453,993
S355_L_8_PULS_07	0.1	342	349,009
S355_L_8_PULS_08	0.1	342	800,043
S355_L_8_PULS_09	0.1	324	5,000,000
S355_A_20_01	0.1	378	113,359
S355_A_20_02	0.1	378	156,630
S355_A_20_03	0.1	378	121,808
S355_A_20_04	0.1	342	264,989

Table 5 (continued)

Test specimen [index]	Load ratio [−]	Nominal stress range [MPa]	Fatigue life [cycles]
S355_A_20_05	0.1	342	381,471
S355_A_20_06	0.1	342	431,486
S355_A_20_07	0.1	306	582,597
S355_A_20_08	0.1	306	861,479
S355_A_20_09	0.1	306	599,853
S355_A_20_10	0.1	252	2,556,693
S355_A_20_11	0.1	252	900,809
S355_A_20_12	0.1	252	1540000*
S355_A_20_13	0.1	216	793326*
S355_A_20_14	0.1	216	5,000,000
S355_A_20_v2_01	0.1	360	138,852
S355_A_20_v2_02	0.1	360	173,888
S355_A_20_v2_03	0.1	324	425,448
S355_A_20_v2_04	0.1	324	381,537
S355_A_20_v2_05	0.1	288	517,881
S355_A_20_v2_06	0.1	288	517,229
S355_A_20_v2_07	0.1	252	927,000
S355_A_20_v2_08	0.1	252	590,000
S355_A_20_v2_09	0.1	216	1,324,000
S355_A_20_v2_10	0.1	216	1,524,000
S355_A_20_v2_11	0.1	216	5,000,000
S355_P_20_01	0.1	396	99,675
S355_P_20_02	0.1	396	114,292
S355_P_20_03	0.1	360	155,701
S355_P_20_04	0.1	360	158,926
S355_P_20_05	0.1	324	558,232
S355_P_20_06	0.1	324	526,026
S355_P_20_07	0.1	306	686,243
S355_P_20_08	0.1	306	807,696
S355_P_20_09	0.1	297	996,650
S355_P_20_10	0.1	297	5,000,000
S355_P_20_11	0.1	288	5,000,000
S355_P_20_v2_01	0.1	360	135,226
S355_P_20_v2_02	0.1	360	114,297
S355_P_20_v2_03	0.1	324	384,991
S355_P_20_v2_04	0.1	324	483,898
S355_P_20_v2_05	0.1	306	536,470
S355_P_20_v2_06	0.1	306	315,000
S355_P_20_v2_07	0.1	270	800,082
S355_P_20_v2_08	0.1	270	5,000,000
S460_A_8_01	0.1	450	142,664
S460_A_8_02	0.1	450	155,522
S460_A_8_03	0.1	396	297,171
S460_A_8_04	0.1	396	295,406
S460_A_8_05	0.1	324	557,191
S460_A_8_06	0.1	324	482,062
S460_A_8_07	0.1	324	709,823
S460_A_8_08	0.1	306	687,746

Table 5 (continued)

Test specimen [index]	Load ratio [−]	Nominal stress range [MPa]	Fatigue life [cycles]
S460_A_8_09	0.1	306	613,861
S460_A_8_10	0.1	288	5,000,000
S690_A_8_01	0.1	216	5,000,000
S690_A_8_02	0.1	216	816354*
S690_A_8_03	0.1	252	578,544
S690_A_8_04	0.1	252	1,509,115
S690_A_8_05	0.1	252	1,158,973
S690_A_8_06	0.1	288	1,053,707
S690_A_8_07	0.1	288	605,269
S690_A_8_08	0.1	288	1,442,738
S690_A_8_09	0.1	324	482,980
S690_A_8_10	0.1	324	608,066
S690_A_8_11	0.1	360	400,725
S690_A_8_12	0.1	360	391,707
S690_A_8_13	0.1	396	249,321
S690_A_8_14	0.1	396	195,460
S690_P_8_01	0.1	324	5,000,000
S690_P_8_02	0.1	324	637,048
S690_P_8_03	0.1	324	422,821
S690_P_8_04	0.1	360	403,119
S690_P_8_05	0.1	360	399,922
S690_P_8_06	0.1	396	205,484
S690_P_8_07	0.1	396	257,007
S690_P_8_08	0.1	432	206,687
S690_P_8_09	0.1	432	155,691
S690_L_8_01	0.1	432	173,579
S690_L_8_02	0.1	432	171,234
S690_L_8_03	0.1	396	227,804
S690_L_8_04	0.1	396	231,498
S690_L_8_05	0.1	342	337,710
S690_L_8_06	0.1	342	297,959
S690_L_8_07	0.1	324	439,918
S690_L_8_08	0.1	324	568,368
S690_L_8_09	0.1	315	471,126
S690_L_8_10	0.1	306	553,959
S690_L_8_11	0.1	306	574,489
S690_L_8_12	0.1	306	2539532*
S690_L_8_13	0.1	288	5,000,000
S690_L_8_PULS_01	0.1	414	182,510
S690_L_8_PULS_02	0.1	396	165,485
S690_L_8_PULS_03	0.1	378	258,820
S690_L_8_PULS_04	0.1	342	285,534
S690_L_8_PULS_05	0.1	342	206,053
S690_L_8_PULS_06	0.1	306	254,324
S690_L_8_PULS_07	0.1	306	379,815
S690_L_8_PULS_08	0.1	288	468,418
S690_L_8_PULS_09	0.1	288	374,260
S690_L_8_PULS_10	0.1	288	569,652

Table 5 (continued)

Test specimen [index]	Load ratio [−]	Nominal stress range [MPa]	Fatigue life [cycles]
S690_L_8_PULS_11	0.1	288	865,773
S690_L_8_PULS_12	0.1	270	5,000,000
S690_A_20_01	0.1	288	5,000,000
S690_A_20_02	0.1	288	995,698
S690_A_20_03	0.1	288	975,552
S690_A_20_04	0.1	324	445,482
S690_A_20_05	0.1	324	565,063
S690_A_20_06	0.1	342	457,415
S690_A_20_07	0.1	360	344,273
S690_A_20_08	0.1	360	353,763
S690_A_20_09	0.1	396	258,100
S690_A_20_v2_01	0.1	360	221,073
S690_A_20_v2_02	0.1	360	251,292
S690_A_20_v2_03	0.1	324	366,979
S690_A_20_v2_04	0.1	288	598,118
S690_A_20_v2_05	0.1	252	641,768
S690_A_20_v2_06	0.1	252	985,738
S690_A_20_v2_07	0.1	234	887,104
S690_A_20_v2_08	0.1	234	1,400,394
S690_A_20_v2_09	0.1	216	5,000,000
S690_P_20_01	0.1	414	160,644
S690_P_20_02	0.1	414	299,981
S690_P_20_03	0.1	396	321,706
S690_P_20_04	0.1	360	420,737
S690_P_20_05	0.1	324	552,437
S690_P_20_06	0.1	324	631,443
S690_P_20_07	0.1	324	915,115
S690_P_20_08	0.1	306	5,000,000
S690_P_20_v2_01	0.1	450	188,121
S690_P_20_v2_02	0.1	450	261,013
S690_P_20_v2_03	0.1	414	293,646
S690_P_20_v2_04	0.1	414	282,224
S690_P_20_v2_05	0.1	360	304,028
S690_P_20_v2_06	0.1	360	446,287
S690_P_20_v2_07	0.1	324	494,507
S690_P_20_v2_08	0.1	324	756,164
S690_P_20_v2_09	0.1	306	5,000,000
S960_A_8_01	0.1	432	149,214
S960_A_8_02	0.1	432	128,565
S960_A_8_03	0.1	360	300,556
S960_A_8_04	0.1	360	317,639
S960_A_8_05	0.1	306	451,014
S960_A_8_06	0.1	306	1,873,188
S960_A_8_07	0.1	306	1,319,542
S960_A_8_08	0.1	288	680,134
S960_A_8_09	0.1	288	632,065
S960_A_8_10	0.1	288	5,000,000

*not included in the calculation

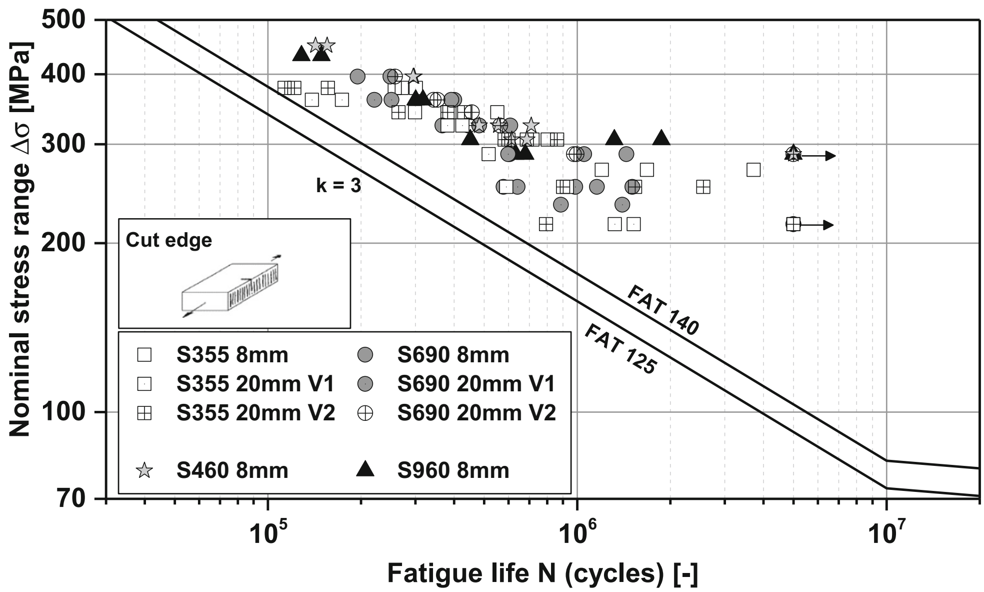

Fig. 11 Fatigue test results oxygen cut edges, 8-mm- and 20-mm-thick specimen, stress ratio $R = 0.1$

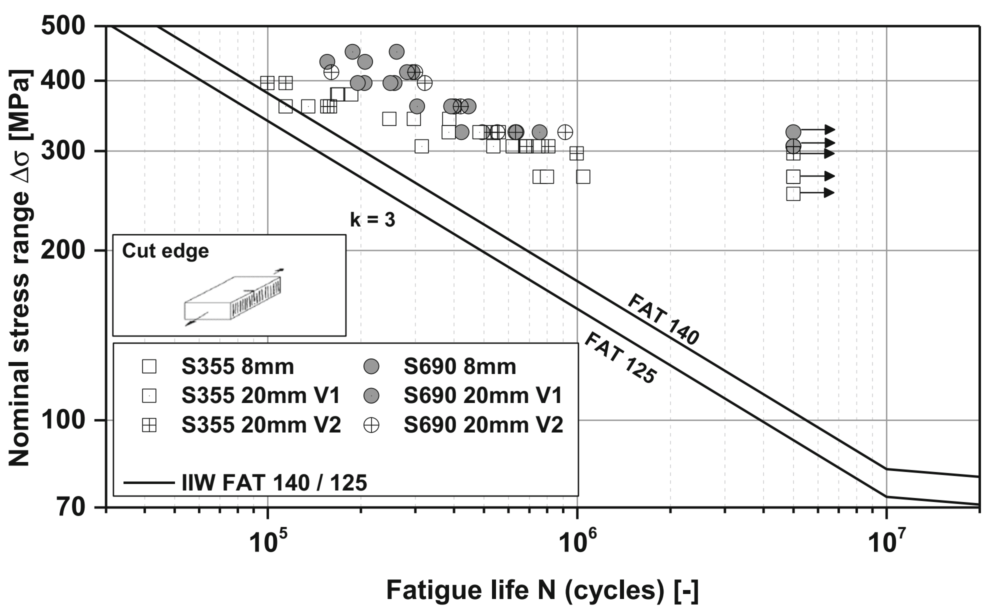

Fig. 12 Fatigue test results plasma cut edges, 8-mm- and 20-mm-thick specimen, stress ratio $R = 0.1$

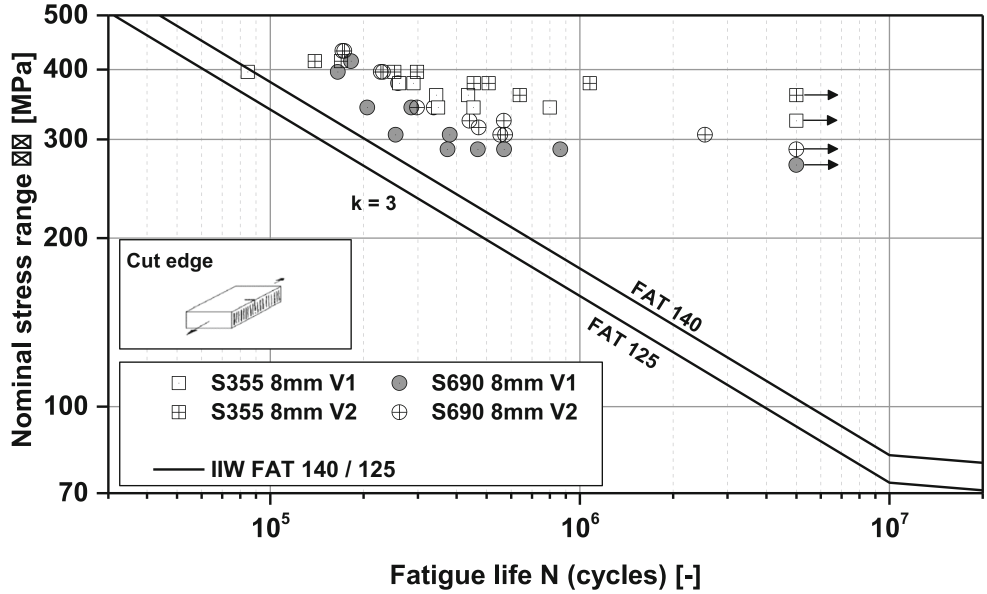

Fig. 13 Fatigue test results laser cut edges, 8-mm- and 20-mm-thick specimen, stress ratio $R = 0.1$

Publisher's Note Springer Nature remains neutral with regard to jurisdictional claims in published maps and institutional affiliations.

References

1. DIN EN 1090 (2017) Execution of steel structures and aluminum structures – Part 2: technical requirements for steel structures; German and English version EN 1090-2
2. DIN EN ISO 9013 (2014) Thermal cutting – Classification of thermal cuts - Geometrical product specification and quality tolerances (ISO/DIS 9013). Beuth Verlag, Berlin
3. Grubisic V, Sonsino CM (1992) Influences of the fatigue strength of forged components, special print VDI-Z Bd 134, (in German)
4. Fuchs HO, Stephens RJ (1980) Metal fatigue in engineering. John Wiley, New York
5. Hempel M (1962) Fatigue behavior of the materials. VDI-Z. 104. 27, 1362–1377, (in German)
6. DIN EN ISO 18265 (2013) Testing of metallic materials - Conversion of hardness values. CEN-CENELEC Management Centre, Brussels
7. Radaj D, Vormwald M (2007) Fatigue strength - fundamentals for engineers, 3. Auflage, Springer Verlag. (in German)
8. Dahl W (1974) Fundamentals of strength and fracture behavior. Verlag Stahleisen, Düsseldorf (in German)
9. Wu Z, Huang Y (2017) Mechanical behavior and fatigue performance of austenitic stainless steel under consideration of martensitic phase transformation. Mater Sci Eng A 679:249–257
10. FKM-Guidelines (2002) Calculated proof of strength for machine components made of steel, cast iron and aluminum materials, 4. Ausgabe. VDMA-Verlag, Frankfurt/M
11. Sperle J-O (2007) Influence of parent metal strength on the fatigue strength of parent material with machined and thermally cut edges. IIW Document XIII-2174-07. International Institute of Welding, Paris
12. Remes H, Korhonen E, Lehto P, Romanoff J, Niemelä A, Hiltunen P, Kontkanen T (2013) Influence of surface integrity on the fatigue strength of high-strength steels. J Constr Steel Res 89(9):21–29
13. Stenberg T, Lindgren E, Barsoum Z, Barmicho I (2016) Fatigue assessment of cut edges in high strength steel - influence of surface quality. KTH Royal Institute of Technology
14. Hobbacher A (2009) IIW recommendations for fatigue design of welded joints and components WRC. Welding Research Council Bulletin, WRC 520, London
15. DIN EN 10025-4 (2011) Hot rolled products of structural steels – Part 4: technical delivery conditions for thermomechanical rolled weldable fine grain structural steels; German version EN 10025-4
16. DIN EN 10025-3 (2011) Hot rolled products of structural steels – Part 3: technical delivery conditions for normalized/normalized rolled weldable fine grain structural steels; German version EN 10025-3
17. DIN EN 10025-5 (2011) Hot rolled products of structural steels – Part 5: technical delivery conditions for structural steels with improved atmospheric corrosion resistance; German version EN 10025-5
18. DIN EN ISO 4288 (1996) Geometrical Product Specifications (GPS) – Surface texture: Profile method – Rules and procedures for assessment of surface texture (ISO 4288)
19. DIN EN ISO 6507-1 (2016) Metallic materials – Vickers hardness test – Part 1: test method (ISO/DIS 6507-1)
20. DIN 50100 (2015) Load controlled fatigue testing – Execution and evaluation of cyclic tests at constant load amplitudes on metallic specimens and components